Bulletin of the Seismological Society of America, Vol. 104, No. 4, pp. 2043–2059, August 2014, doi: 10.1785/0120140032

Seismic-Wave Attenuation Determined from Tectonic Tremor in Multiple Subduction Zones

by Suguru Yabe, Annemarie S. Baltay, Satoshi Ide, and Gregory C. Beroza

Abstract Tectonic tremor provides a new source of observations that can be used to constrain the seismic attenuation parameter for ground-motion prediction and hazard mapping. Traditionally, recorded earthquakes of magnitude ~3–8 are used to develop ground-motion prediction equations; however, typical earthquake records may be sparse in areas of high hazard. In this study, we constrain the distance decay of seismic waves using measurements of the amplitude decay of tectonic tremor, which is plentiful in some regions. Tectonic tremor occurs in the frequency band of interest for ground-motion prediction (i.e., ~2–8 Hz) and is located on the subducting plate interface, at the lower boundary of where future large earthquakes are expected. We empirically fit the distance decay of peak ground velocity from tremor to determine the attenuation parameter in four subduction zones: Nankai, Japan; Cascadia, United States–Canada; Jalisco, Mexico; and southern Chile. With the large amount of data available from tremor, we show that in the upper plate, the lower crust is less attenuating than the upper crust. We apply the same analysis to intraslab events in Nankai and show the possibility that waves traveling from deeper intraslab events experience more attenuation than those from the shallower tremor due to ray paths that pass through the subducting and highly attenuating oceanic crust. This suggests that high pore-fluid pressure is present in the tremor source region. These differences imply that the attenuation parameter determined from intraslab earthquakes may underestimate ground motion for future large earthquakes on the plate interface.

Introduction

Subduction zone earthquakes represent a large hazard for society. Accurate ground-motion prediction, for hazard mapping and decision making, can help mitigate the disaster caused by these events. Ground-motion prediction equations (GMPEs) express ground motion primarily as a function of magnitude and distance, but usually also as a function of parameters such as mechanism, depth, and site classification (e.g., Boore and Joyner, 1982; Si and Midorikawa, 2000). GMPEs are developed using recordings of moderate to large earthquakes in the area of interest. However, in some subduction zones, such as Nankai and Cascadia, the usual seismicity on the plate interface is quite low, which makes it difficult to empirically constrain the parameters in GMPEs, despite the evident risk of great earthquakes (Ando, 1975; Satake *et al.*, 1996).

Tectonic tremor is common in both the Nankai and Cascadia subduction zones (Obara, 2002; Rogers and Dragert, 2003). It is thought to occur as shear slip on the subducting plate interface beneath the lower edge of the coupling zone of great earthquakes (Shelly *et al.*, 2006; Ide, Shelly, and Beroza, 2007; Chapman and Melbourne, 2009; Liu *et al.*, 2010; Royer and Bostock, 2013). Therefore, seismic waves from tectonic tremor should experience attenuation similar to that of waves from plate-interface great earthquakes. Although tectonic tremor is primarily detected in the frequency band between 2 and 8 Hz (Obara, 2002), and the amplitude of tremor is much smaller than that recorded from modest ordinary earthquakes, Baltay and Beroza (2013) showed that records of tectonic tremor can be used to constrain the seismic attenuation parameter within this frequency range. This study expands on that work to estimate attenuation in several different subduction zones with an improved, simultaneous inversion for the source, path, and site.

Estimating seismic attenuation in this manner is useful for ground-motion prediction, but it also elucidates our understanding of the conditions for tectonic tremor genesis, as attenuation is sensitive to the presence of fluids. The existence of high pore-fluid pressure around tremor hypocenters has been proposed by seismic imaging studies (Shelly *et al.*, 2006; Hirose *et al.*, 2008; Audet *et al.*, 2009; Kato *et al.*, 2010). Other studies demonstrate that tremor activity is susceptible to small stress changes generated by tide and surface waves from distant earthquakes, which suggests that tremor occurs on very weak fault planes with high-pressured pore fluid (e.g., Miyazawa and Mori, 2005; Shelly *et al.*, 2007; Thomas *et al.*, 2009). Petrology studies suggest that the fluid may be supplied by the dehydration reaction of hydrated

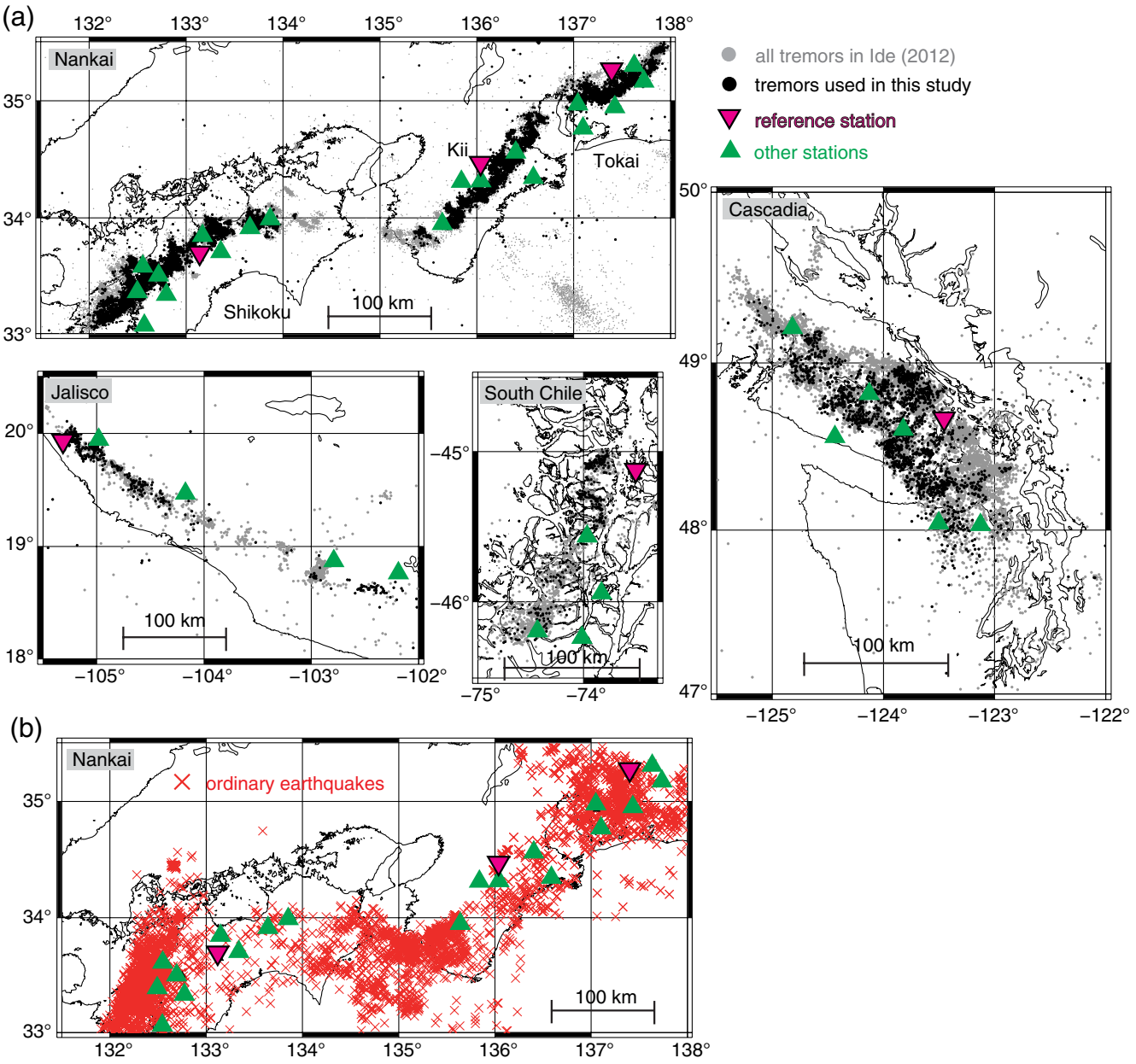

Figure 1. (a) The distribution of tectonic tremor used in this study, in six regions in four subduction zones (Shikoku, Kii, and Tokai in the Nankai subduction zone; the Cascadia subduction zone near southern Vancouver Island; the Jalisco region in Mexico; and southern Chile north of the triple junction), as detected and located by Ide (2012). All tremor considered is shown with light gray dots; tremor actually used for the analysis (after the noise threshold is considered) is plotted in black dots. Selected stations are shown with triangles, and a reference station for site factors in each region is indicated with an inverted triangle. (b) In three regions in the Nankai subduction zones, the intraslab earthquakes used for analysis are shown with crosses among ordinary earthquakes in the Japan Meteorological Agency (JMA) catalog. The color version of this figure is available only in the electronic edition.

minerals in the subducting oceanic crust (Peacock and Wang, 1999; Hacker *et al.*, 2003), which may have very low seismic velocity and high V_P/V_S ratio (Eberhart-Phillips *et al.*, 1989), as seen in seismic imaging studies (Shelly *et al.*, 2006; Hirose *et al.*, 2008; Audet *et al.*, 2009; Kato *et al.*, 2010). Such oceanic crust should also be strongly attenuating, as detected in some tomography studies (Winkler and Murphy, 1995; Eberhart-Phillips *et al.*, 2005; Reyners and Eberhart-Phillips, 2009; Takaoka *et al.*, 2012; Kita *et al.*, 2013). Here, we also discuss the existence of a strongly attenuating layer beneath the plate interface on which tremor occurs.

We estimate the seismic attenuation parameter in six regions: Shikoku, Kii, and Tokai in the Nankai subduction zone in southwest Japan; the southern region of Vancouver Island in the Cascadia subduction zone; the Jalisco region in Mexico; and the northern region of the triple junction formed by the Nazca, South American, and Antarctic plates in southern Chile (Fig. 1). We use the timing and locations

of tremor as cataloged in each of these regions (Ide, 2012) to investigate the seismic attenuation. We also apply the same inversion method to ordinary earthquakes in the Nankai subduction zone using the Japan Meteorological Agency (JMA) catalog, which consists of small intraslab earthquakes occurring 5–10 km below the plate interface, which is likely near the oceanic Moho. By comparing the attenuation parameter obtained from tectonic tremor with that from these intraslab earthquakes, we can constrain the attenuation structure in the subducting oceanic crust.

Tectonic Tremor Peak Ground Velocities

We use the tremor catalog provided by Ide (2012), which describes timing, duration, and locations of individual tremor events, determined using an envelope correlation method (Ide, 2010) and shown for the six regions in Figure 1a. In total, nearly 70,000 tremor events are considered (Table 1). Except for Nankai, where the noise level is relatively low, only events occurring at night (from 8 p.m. to 7 a.m. at the local time) are used in the analysis to reduce the effects of anthropogenic noise (e.g., Baltay and Beroza, 2013). Although the majority of the events in the Ide (2012) catalog are tectonic tremor, a few ordinary earthquakes are also included, especially offshore of Nankai and along the southern Chile coast, which we manually remove from the catalog. To reduce potential outliers, the occasional time periods during which several tremor events occur simultaneously, yet in different locations, are removed.

The hypocentral distance and peak ground velocity (PGV) of velocity waveforms are measured for each event–station pair used in our analysis. The hypocentral distance is determined from the epicentral distance of the event from the catalog location to the station location, with an assumed depth of 30 km because depth estimated by envelope correlation method is less certain. Continuous velocity waveforms are downloaded from Hi-net for the Nankai region, from Incorporated Research Institutions for Seismology (IRIS) and Canadian National Data server (CNDC) for Cascadia, and from IRIS for other regions (see Data and Resources for details). Waveforms are band-pass filtered between 2 and 8 Hz, and the two horizontal components are summed in a vector sense. Based on the origin time of events and the *S*-wave travel time calculated from the seismic-velocity structure of Ueno *et al.* (2002), JMA 2001, we calculate the *S*-wave arrival time for each event–station pair. The center of a time window is set to this arrival time, with the total length of the window equal to the duration of the tremor event as determined by Ide (2012). PGV is then measured as the maximum amplitude of the vector-summed record in the time window for each event–station pair.

Because of the extremely small amplitudes of the tremor signal, it is essential to use stations with good signal-to-noise ratio. At each station, we define the noise threshold, below which we reject any PGV measurements. To determine this noise threshold, we make PGV measurements at each station over 20 s time windows that are randomly selected at many times during quiet days (Fig. 2). A quiet day is when there is no known tremor within 300 km of the station nor ordinary earthquakes larger than magnitude 4. In Nankai and Jalisco, we use the regional earthquake catalogs of JMA and of Universidad Nacional Autonoma de Mexico (UNAM), respectively; in Cascadia and southern Chile, there are few earthquakes larger than magnitude 4 nearby, so we assume there is no earthquake contamination. The noise threshold of PGV is measured as the 95th and 99th percentiles of the distribution of noise PGVs, for weaker and stricter thresholds, respectively (Fig. 2a). In Jalisco and southern Chile, the weaker (95th percentile) threshold is used due to the small number of events in the tremor catalog, whereas the stricter threshold is used in Nankai and Cascadia; however, we also test the weaker threshold during error estimation.

Figure 2 compares typical examples of quiet and less well-recorded stations (i.e., noisier or farther stations) in Shikoku. We see that, for a quiet station, many PGV measurements are above the noise threshold and can be used in the analysis, whereas most PGV values are below the threshold at a less well-recorded station. Therefore, the range of PGV is wide for a quiet station, and we can readily observe the decay of PGV with distance (Fig. 2b). This trend is not observable for a less well-recorded station because there are too few PGV measurements, and hence stations such as this are not used. Based on the noise thresholds and availability of velocity data, we selected 5–10 stations for each region, shown in Figure 1. Hereafter, only events at these selected stations with PGVs above the noise threshold are used for analysis.

Table 1
Tremor Catalog (Ide, 2012) for the Estimation of Seismic Attenuation Parameter

Region	Dates (yyyy/mm)	Number of Events in the Catalog	Number of Events Used in the Analysis
Shikoku	2004/04–2009/03	26,500	10,800
Kii	2004/04–2009/03	11,800	4500
Tokai	2004/04–2009/03	9700	4000
Cascadia	2005/01–2009/12	10,200	2100
Jalisco	2006/01–2007/06	1500	400
Southern Chile	2005/01–2007/01	2200	400

Data: Intraslab Earthquakes Peak Ground Velocities

In addition to using tremor velocity data, we also test the method on intraslab earthquakes in the Nankai subduction zone. These events are in the JMA catalog with depths between 30 and 50 km and JMA magnitudes from 1 to 3, and they occur between April 2004 and December 2007 (Fig. 1b). The method for processing the velocity data for these intraslab earthquakes is the same as that for the tremor events (i.e., 2–8 Hz frequency range); however, the earthquake depth from the JMA catalog is used to determine the hypocentral distance, and a fixed 20 s time window centered

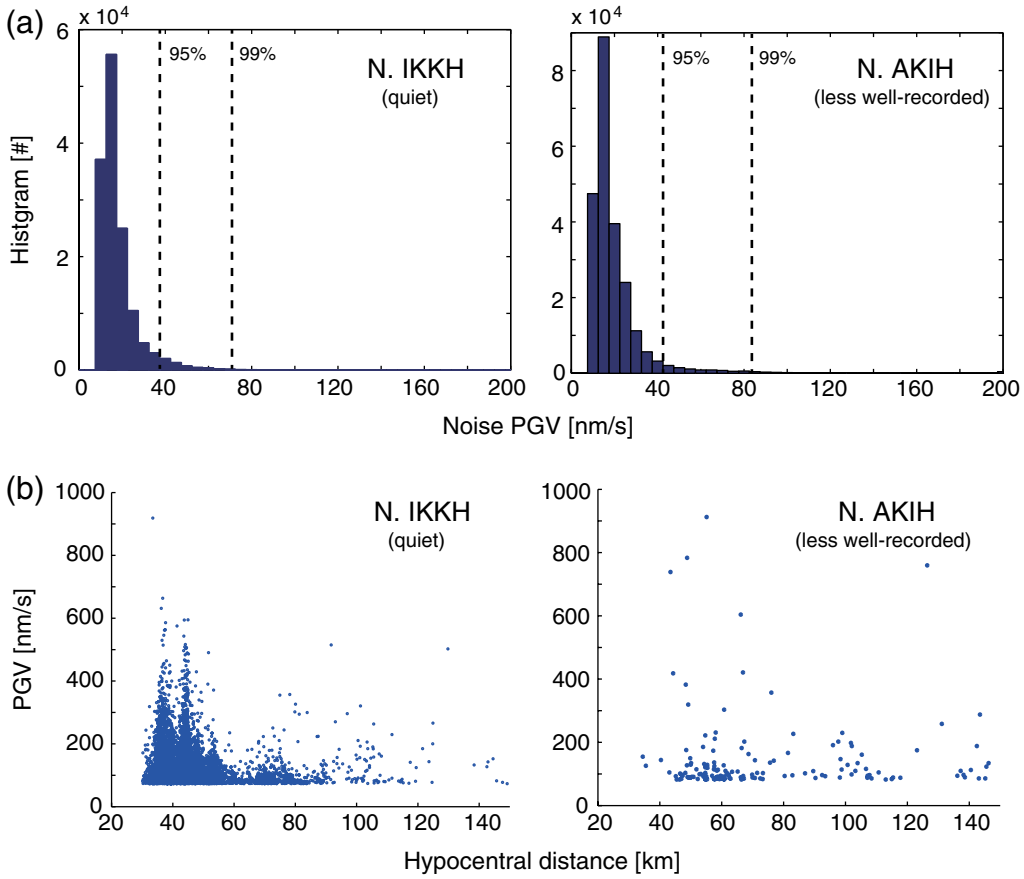

Figure 2. Example of a quiet station and a less well-recorded station in Shikoku. (a) Histogram of noise peak ground velocity (PGV) measured on a quiet day (see Tectonic Tremor Peak Ground Velocities section) shown for a quiet station (left, N. IKKH) and a less well-recorded station (right, N. AKIH). Two dashed lines indicate the defined weaker (95th percentile) and more strict (99th percentile) noise thresholds for each station. (b) Measured PGV for tectonic tremor plotted against hypocentral distance. Left panel shows the example of the quiet station (N. IKKH), showing larger amplitude at close distance; the right shows the less well-recorded station (N. AKIH), with only a small number of signals above the noise threshold. The color version of this figure is available only in the electronic edition.

on the *S*-wave arrival time is used for the PGV measurement. Although we do not model radiation patterns in this study, we note that some intraslab events might be strike slip, in which case stations that are directly above the events may be near a nodal plane for the *S*-wave radiation pattern, even for frequencies above ~1 Hz (Obana *et al.*, 2005; Takemura *et al.*, 2009; Miyoshi and Obara, 2010). To avoid this complication, we discard records from intraslab earthquakes with hypocentral distances less than 50 km only in the Tokai region.

Method: Simultaneous Estimation for Attenuation Parameter and Site Factors

We extend the method of Baltay and Beroza (2013) to estimate the seismic attenuation parameter for GMPEs using tremor. Here, we perform a simultaneous inversion to estimate the attenuation parameter and site factors at the same time, using the hypocentral distance and PGV as described previously.

The simple GMPE used in this method can be expressed as the source amplitude combined with geometrical spreading, path attenuation, and the site response:

$$A_{ij} \sim \text{Source}_i \times \frac{1}{R_{ij}} \times \exp(-CR_{ij}) \times \text{Site}_j, \qquad (1)$$

for the ith event and jth station, in which the measured amplitude A_{ij} is PGV. Source_i is the source term for the ith event, usually expressed as a function of the moment magnitude. Typical GMPEs also consider effects of source mechanism, but here we do not include this effect as we assume that seismic waves are scattered once they travel more than a few tens of kilometers (e.g., Takemura *et al.*, 2009). R_{ij} is the hypocentral distance with $1/R$ representing the geometrical spreading of the body wave in a homogeneous medium. When the hypocentral distance becomes large, the surface waves become more dominant, and geometrical spreading is ideally $1/\sqrt{R}$. Though this crossover distance (the point at which the geometrical spreading deviates from $1/R$) is suggested to be about 50 km for crustal earthquakes (Boatwright and Seekins, 2011), we consider $1/R$ as the

geometrical spreading out to 150 km, the full range of our data. Because tectonic tremor occurs deeper than crustal earthquakes, the crossover distance should be larger. Our estimated seismic attenuation should be correct as the first-order approximation because we only use data within 150 km; however, if the geometrical spreading is indeed less strong, we would underestimate the seismic attenuation. C is the attenuation parameter that we seek, defined as $C = \pi f/Q\beta$ when considering a specific frequency, so that $\exp(-CR_{ij})$ includes both seismic attenuation by anelastic effects and the effect of scattering. In this study, C represents the seismic attenuation of the dominant PGV frequency between 2 and 8 Hz. Furthermore, we assume a homogeneous attenuation structure for simplicity, so that the obtained attenuation parameters represent path-averaged attenuation, although in reality the attenuation structure will have 3D structure in each region. Site_j in equation (1) is the site-response factor for the jth station, which reflects the seismic structure at very shallow depths and may consist of amplification, attenuation, and nonlinear soil effects.

Magnitude determination of individual tectonic tremor events is difficult due to the small amplitudes and emergent signal and is not routinely calculated for all of the events in the catalog. Without this magnitude information, we cannot constrain the source term in equation (1). To avoid this problem, we compare equation (1) for the ith event, recorded at two stations, j and k, after taking the natural logarithm:

$$\log(A_{ij} \times R_{ij}) - \log(A_{ik} \times R_{ik}) = -C(R_{ij} - R_{ik}) + [\log(\text{Site}_j) - \log(\text{Site}_k)] + e_{ijk}, \quad (2)$$

in which e_{ijk} represents error. By taking the amplitude difference for one event recorded at two stations, the common source term cancels. In equation (2), the known parameters are A_{ij} (PGV) and R_{ij} (hypocentral distance), with C (attenuation parameter) and Site_j (the site factor) as the unknown parameters to be determined. Because we can estimate only relative site factors when solving the inverse problem of equation (2), we need one additional assumption about the site factor. Hence, Site_1 is set to be the reference station with a value of 1, and relative station factors are estimated for other stations. The choice of reference station does not have special meaning or significance but is shown in Figure 1.

We solve equation (2) for the attenuation parameter and relative site factors by L1-norm minimization for e_{ijk}. We use L1 minimization rather than L2 minimization to reduce the influence of outliers in data on the estimation. The L1-norm minimization is solved with linear programming (Dantzig *et al.*, 1955; Mehrotra, 1992; Zhang, 1998). To obtain the final results, we solve the same inverse problem again after removing outliers, defined as observations beyond the 3σ level.

Throughout the analysis, we estimated the attenuation parameter within a hypocentral distance limit. We use PGV data with hypocentral distance less than the distance limit, creating all possible pairs between these records (equation 2). We consider that the determined attenuation parameter C represents the averaged attenuation of the region within that hypocentral distance. We test this distance limit, ranging from 50 to 150 km at 10 km interval (except for the Jalisco data, where the smallest hypocentral distance we can consider is 120 km due to sparse station distribution). At shorter hypocentral distances, the ray paths are nearly vertical because the events occur at approximately 30 km depth; for larger hypocentral distances the ray paths become horizontal and sample the deeper layers. For that reason, the estimated C becomes more sensitive to attenuation in deeper layers, as the distance limit increases. By considering the attenuation parameter determined at various distance limits, we can constrain the vertical structure of the attenuation as discussed in the Synthetic Tests for Distance-Dependent Attenuation Parameter from Tectonic Tremor section.

Attenuation and Site Parameters from Tectonic Tremor

Following the inversion scheme outlined above, we use the PGV and hypocentral distance data from tectonic tremor to solve for attenuation parameter C and the relative site terms. We first examine the tremor PGV data (Fig. 3a) to confirm that it shows a decaying trend with distance, which is primarily attributable to geometrical spreading, using the Shikoku data set as an example. The obtained attenuation parameters at each distance limit and the relative site factors at each station are shown in Figure 3b. When using a smaller distance limit, less than ~70 km, the attenuation parameter is larger, whereas use of a larger distance limit causes the attenuation to decrease. C becomes less dependent on the distance limit at larger distances and converges to around 0.008. The site factors are less dependent on the distance limit and are stably obtained. For each parameter, we calculate error bars using a model covariance matrix, in which equation (2) is solved by L2 minimization (e.g., Menke, 1989). The root mean square of the error e_{ijk} is calculated using C and site factors obtained from the L1 minimization. This range approximately represents $\pm 1\sigma$ bounds and is shown in all the figures as error bars, which are sometimes smaller than the symbol size. We compare the initial PGV amplitudes (A_{ij}) corrected by $1/R$ geometrical spreading and site terms to visualize C as the slope of the differences in distance (Fig. 3c):

$$\log(A_{ij} \times R_{ij}) - \log(A_{ik} \times R_{ik}) - \log(\text{Site}_j) + \log(\text{Site}_k) = -C(R_{ij} - R_{ik}) + e_{ijk}. \quad (3)$$

When the distance limit is 50 km (Fig. 3c, panel A), the slope is clearly steeper, implying greater attenuation than when the distance limit is 100 km (Fig. 3c, panel B) or 150 km (Fig. 3c, panel C). With the increase of the distance limit, more data are included at greater distances, and the resulting estimated attenuation represents the averaged seismic attenuation in the larger region.

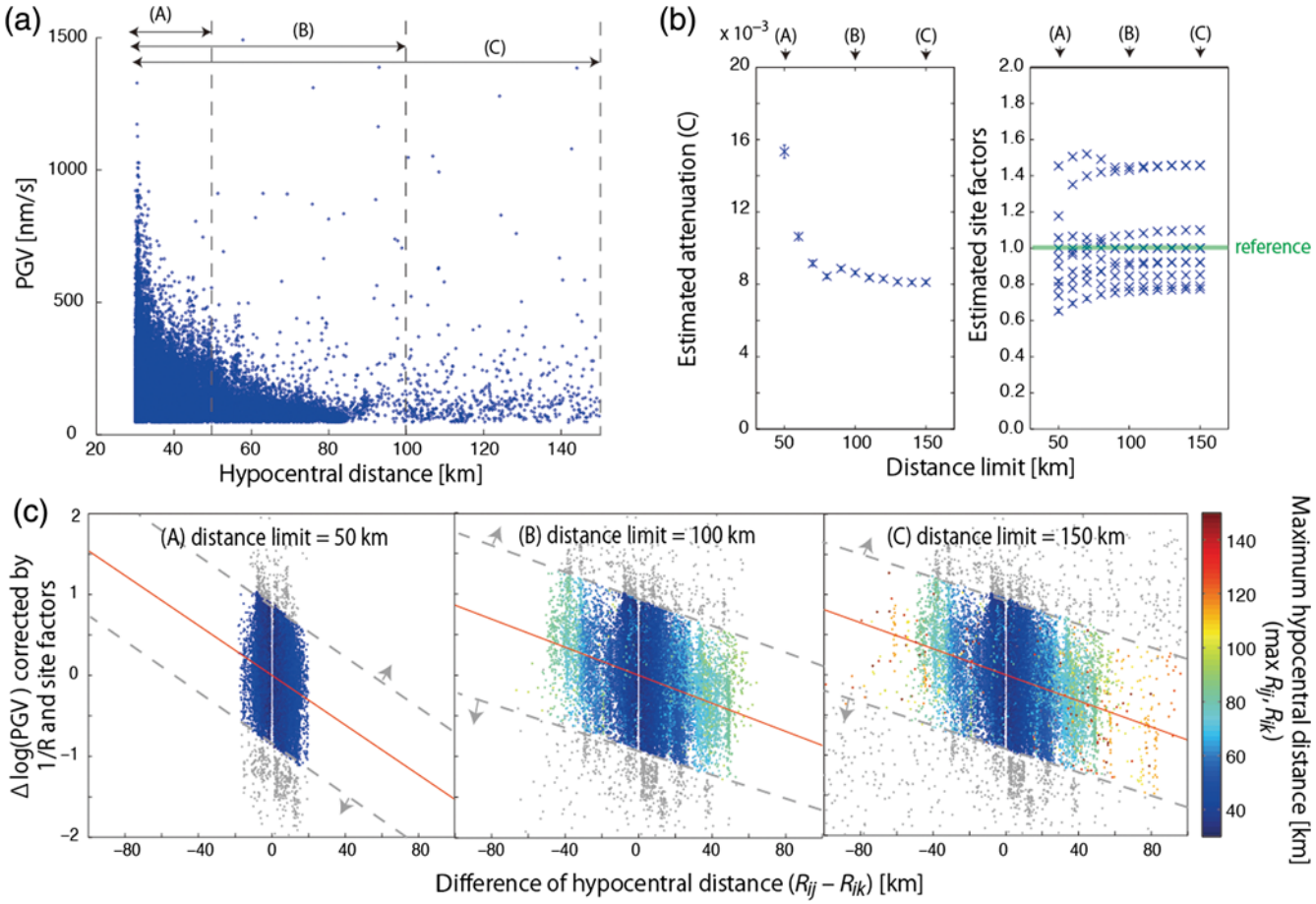

Figure 3. Data and results in the Shikoku region. (a) Measured PGVs of tectonic tremor at selected stations are plotted against hypocentral distance. Three windows, (A), (B), and (C), represent the distance limit of 50, 100, and 150 km, respectively, and correspond with panels (A), (B), and (C) in the lower section of the figure. (b) The estimated attenuation parameter C and site factors for each station are plotted at each distance limit. The solid line shows the station factor of reference station (i.e., 1). (c) The best-fit line, the slope of which is equal to the $-C$ parameter obtained from estimated parameters when the distance limit is (A) 50 km, (B) 100 km, and (C) 150 km, is shown by a solid line. Dashed lines with arrows indicate the approximate level beyond which data are removed when solving the inverse problem the second time because of large scattering ($>3\sigma$). The vertical axis is the amplitude ratio, in log scale, of two stations for the same event corrected with $1/R$ geometrical spreading and estimated station factors. The color version of this figure is available only in the electronic edition.

The attenuation parameter values C obtained in all regions are summarized in Figure 4. The Kii and Jalisco regions have the largest C values (around 0.010), whereas Tokai, Cascadia, and southern Chile have relatively smaller C values (near 0.006), implying less attenuation along the tremor ray paths. The attenuation parameter value in Shikoku is near 0.008. The reliability of these estimates is about ± 0.002 for C and about $\pm 20\%$ for site factors (see the Error Estimation section). With the exception of the Jalisco region, where we have few data at shorter distances, a trend emerges between regions in that C is larger when the distance limit is small and becomes smaller and less dependent on the limit as the distances limit increase. In comparing these distance-dependent C values with those of Baltay and Beroza (2013) in Cascadia (fig. S5 of Baltay and Beroza, 2013), we find a much stronger dependence, especially for the shorter distances, yet find a similar value for C at farther distances. One reason for this observed difference is that Baltay and Beroza (2013) estimate their final C using equation (1), after obtaining and adjusting for site and source terms from residuals of an initial inversion. Using equation (1) directly for estimating the attenuation parameter tends to give more weight to data at greater distances, compared to using equation (2), which employs differential distances. A second reason for the difference in the distance trend may be use of different stations in the analysis. We include two surface stations (CNDC) in addition to five borehole stations (PBO), whereas Baltay and Beroza (2013) use only the PBO borehole stations. The different set of stations might also reflect regional variations of seismic attenuation.

We can evaluate the source term using equation (1) and substituting in the estimated C and site factors (Fig. 5) calculated at a distance limit of 150 km. In each region, the source terms have a lognormal or skew lognormal

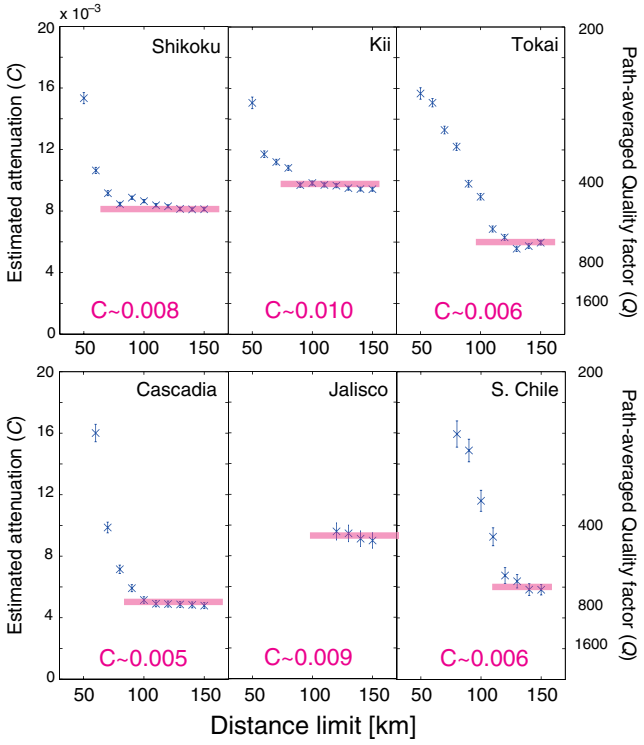

Figure 4. The estimated attenuation (C) in all regions is plotted at each distance limit. The solid line shows stable C values determined at the larger distance limits in each region, reported in Table 2. On the right vertical axis, approximate path-averaged quality factors Q are shown as well, which are calculated by $C = \pi f / Q\beta$ with $\beta = 3.5$ km/s and $f = 4.5$ Hz (the middle of the frequency range of tectonic tremor). The color version of this figure is available only in the electronic edition.

distribution, similar to that found by Baltay and Beroza (2013) in Cascadia. Although typical values for the source term differ between regions, physical interpretation of these values requires care because the absolute amplitude of the reference site in each region is not constrained.

Attenuation and Site Parameters from Intraslab Earthquakes

In the three regions in the Nankai subduction zone (Shikoku, Kii, and Tokai), we apply the previously described method to PGV of intraslab earthquakes. Comparing the results of C from both the intraslab earthquakes and tectonic tremor (Fig. 6), we see that C from tremor is much smaller and statistically significant as the error bars do not overlap. Although care should be taken when comparing these attenuation values due to the different frequency content between ordinary earthquakes (whose spectra are peaked at the corner frequency) and that of tectonic tremor (whose frequency spectrum is flat in the 2–8 Hz range; Ide, Beroza, *et al.*, 2007), this large difference in C parameters suggests it is a true difference in the path-averaged attenuation for tectonic tremor as compared to intraslab earthquakes. The estimated site factors (Fig. 6a right) are comparable with those from tectonic tremor, within the 20% estimation reliability. Results from the Kii and Tokai regions (Fig. 6b) show a similar trend, with stronger attenuation from intraslab events as compared to tremor. Because the hypocenters of intraslab earthquakes are deeper, presumably in the oceanic mantle, the source of the stronger attenuation is around the subducting oceanic crust. Because we cannot separate the intrinsic attenuation

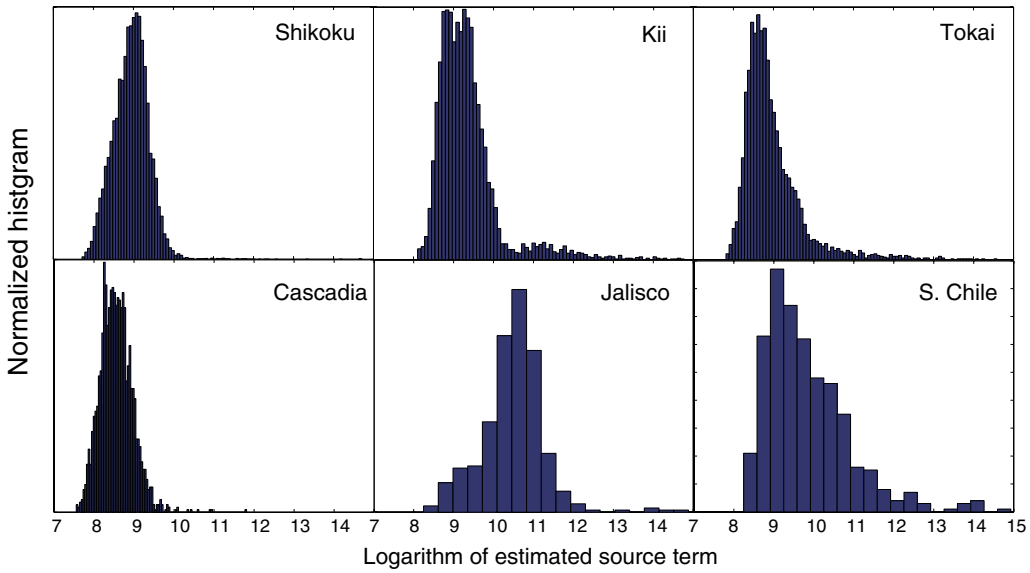

Figure 5. Histograms of the logarithm of source terms are shown for all regions. The source term of tectonic tremor is calculated using equation (1) with A_{ij} in nm/s and R_{ij} in km. The color version of this figure is available only in the electronic edition.

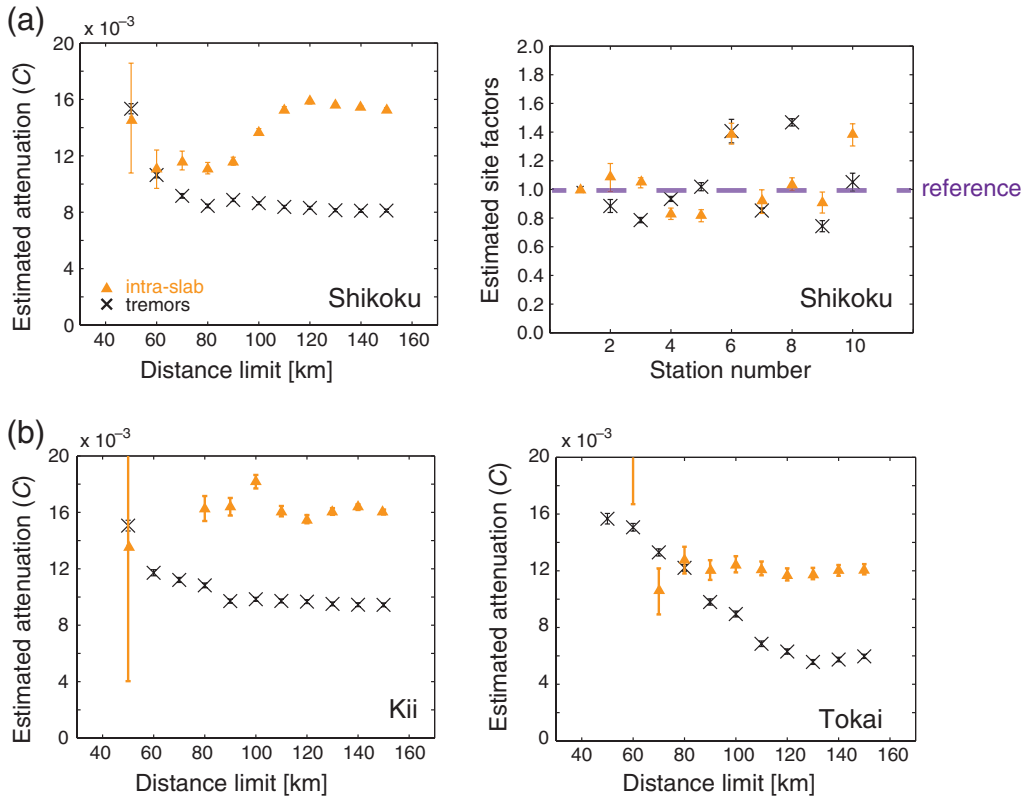

Figure 6. Estimated attenuation and site factors from intraslab earthquakes. (a) (left) Estimated C from intraslab earthquakes (triangles) is compared with the estimated C from tectonic tremor (crosses; Fig. 4) in the Shikoku region. (right) Site factors estimated from intraslab earthquakes (triangles) and tectonic tremor (crosses) are compared in the Shikoku region. The average and standard deviation (shown as error bars) for all distance limits are plotted for each station. (b) Estimated C from tectonic tremor (crosses; Fig. 4) and intraslab earthquakes (triangles) are compared for the (left) Kii and (right) Tokai regions. The color version of this figure is available only in the electronic edition.

from the scattering effect, at least two interpretations exist. The first is that the estimated strong attenuation is due to scattering of the seismic wave at the plate boundary. The second is that an intrinsic attenuating layer exists between the hypocenters of tectonic tremor and that of intraslab earthquakes. We prefer the latter possibility due to the existence of high-pressured fluid near the locations of tectonic tremor and the high attenuation of subducting oceanic crust, as suggested by previous studies (e.g., Eberhart-Phillips *et al.*, 2005; Shelly *et al.*, 2006). However, our results cannot exclude other possibilities, such as the existence of a thin attenuating layer of subducting sediments, as imaged by a multichannel seismic study at the shallow part of subduction zone (Park *et al.*, 2002), as a source of strong attenuation.

Error Estimation

We test the reliability of the attenuation parameter and site-factor estimates through three tests: first, a jackknife test is performed to estimate the error in each region; second, we assess the dependency of the results on selected stations; and third, we examine the sensitivity of the results to the noise criteria used.

To perform the jackknife test for the reliability of the C and site factors, we remove 10% of the data (PGV adjusted for geometrical spreading; the left side of equation 2) and re-estimate the parameters, using L1-norm minimization, as described in the initial analysis. We use a distance limit of 150 km and repeat the Jackknife procedure 100 times in each region. The results are shown in Figure 7 as the histograms of estimated parameters, with estimated values of C in Figure 7a and the estimated site factors in Figure 7b. The ranges of values for the C and site parameters, particularly for the Nankai and Cascadia regions, are small. Because of sparse data in Jalisco and southern Chile, the errors are somewhat larger. In the Jalisco region, two stations have bimodal distribution (indicated by arrows in Fig. 7b) due to the trade-off between these two site factors. This trade-off does not affect the estimate of C, as shown in the Figure 7a.

Because this jackknife test estimates the random error of the mean of the parameters, we also consider the systematic error from each station. We perform a leave-one-out test by removing all data from one station (other than the reference station) and recalculating the attenuation parameter and site factors, again with a distance limit of 150 km. Figure 8 shows some variation in the estimated attenuation parameters when leaving out each station. The amplitudes of the variation are

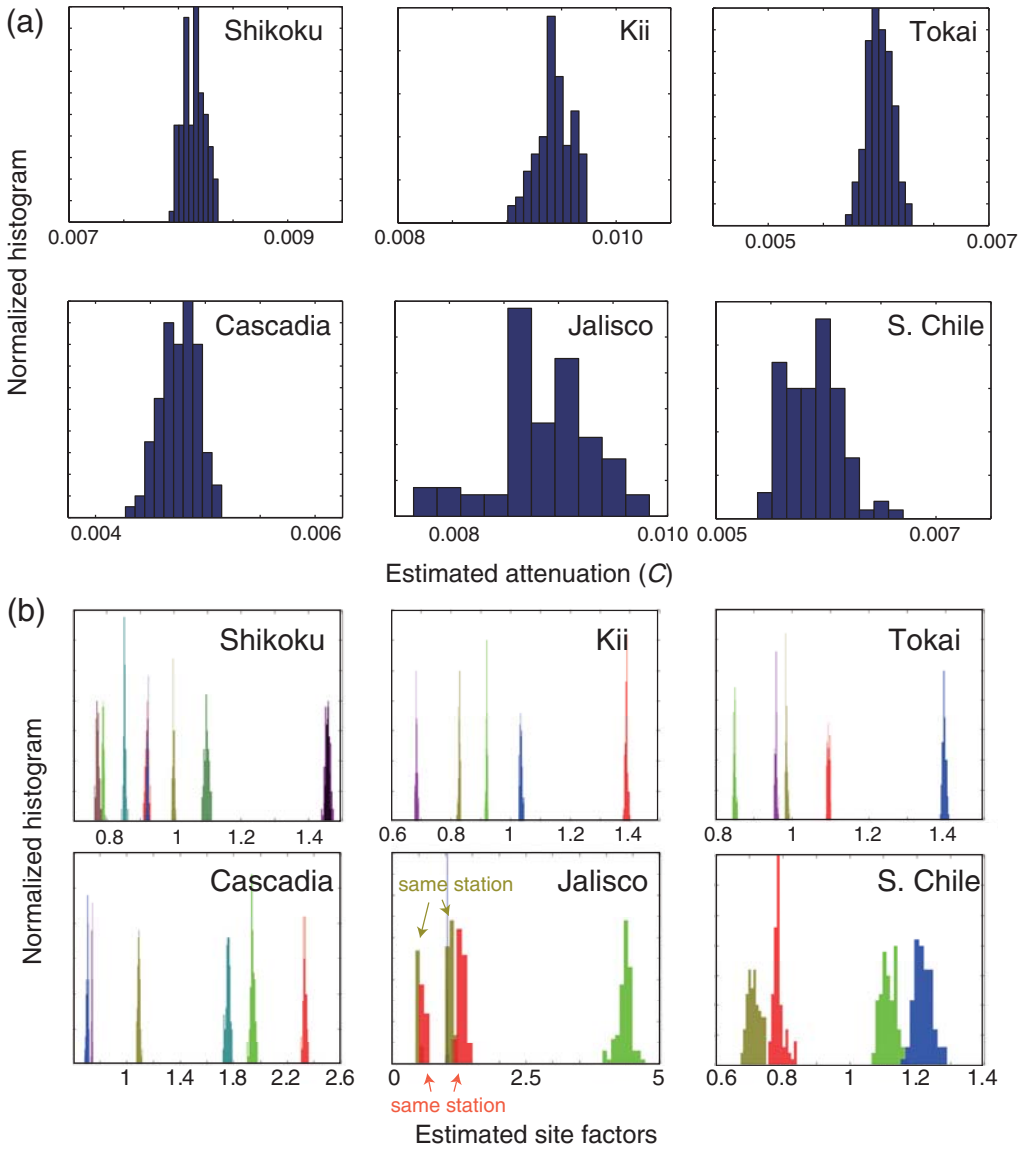

Figure 7. Error estimation through a jackknife test. Seismic attenuation and site factors are re-estimated 100 times, removing 10% of the data randomly each time. (a) Histograms of re-estimated C for all regions from the result of the jackknife test with a distance limit at 150 km. (b) Histograms of estimated site factors for all regions from the same test. Each separate histogram represents a station in that region. The color version of this figure is available only in the electronic edition.

about ± 0.002 for C and $\pm 20\%$ for the site factors. We regard these values as the error of our estimation from this test. There are, however, some stations that cause a significant deviation, which might represent the subregional heterogeneity of the attenuation structure. For example, in the Kii region, C estimated without the northeastern-most station (N.URSH; station 4) is very small. Pei *et al.* (2009) found attenuation in the shallowest 10 km of crust to be relatively high in the northeastern part of the Kii Peninsula, whereas the shallow attenuation is less in the southern part. The dependency of our results on station N.URSH seems consistent with this local distribution of seismic attenuation in the shallow layer. However, because this variation is not visible in the result of Nakamura and Uetake (2002), who estimated the averaged crustal attenuation structure between 0 and 30 km depth, further detailed investigation is necessary to fully understand the cause of the differences.

Finally, we test the dependency of the parameter estimation on the noise criteria threshold, using the Nankai and Cascadia subduction zones, where the data are more plentiful. In Mexico and southern Chile, we use the weaker noise threshold (95th percentile) due to the smaller number of tremor events in the catalog. We compare the results of the estimated C parameter using both the weaker and stronger (99th percentile) noise criteria (Fig. 9). Although the differences are within ± 0.002 for the most part, the deviation is systematic and somewhat larger in the Kii region. This suggests the possibility of systematic errors in the results

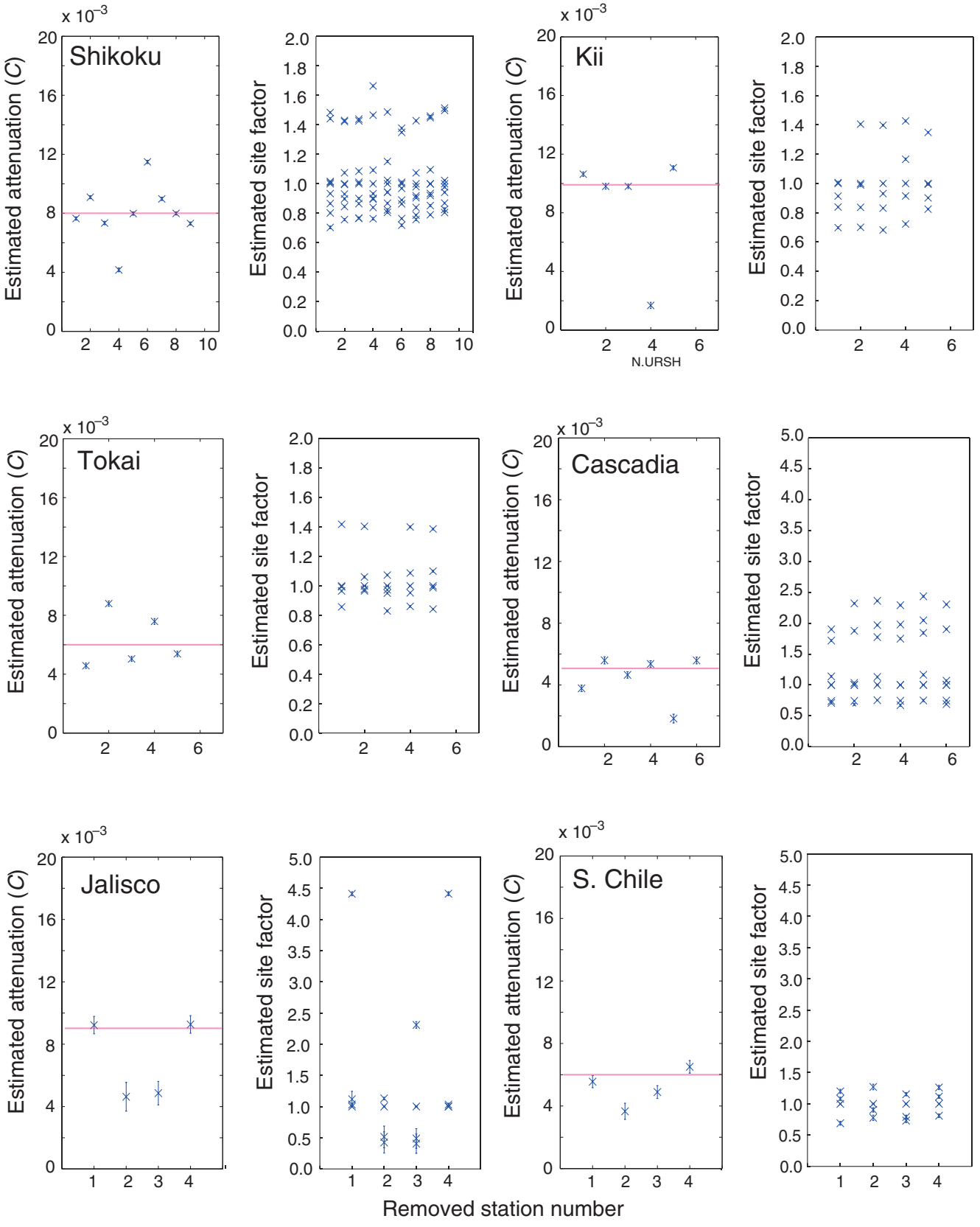

Figure 8. Results from the leave-one-out test for station dependency of the estimated parameters is shown for each region. Estimated C and site factors are re-estimated with a distance limit at 150 km after removing a specific station. The horizontal line in the left panel of each region represents the stable value of estimated C using all stations (Fig. 4). The color version of this figure is available only in the electronic edition.

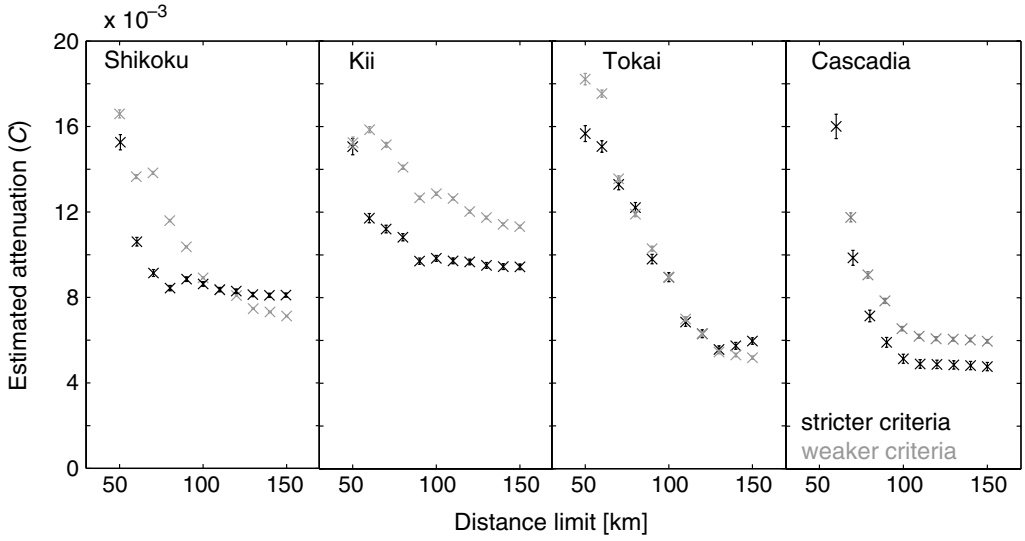

Figure 9. The estimated C with weaker noise criteria is compared with the C with stricter criteria in the Shikoku, Kii, Tokai, and Cascadia regions. The estimated C with stricter criteria plotted in black (99th percentile; same plot as in Fig. 4) and estimated C with weaker criteria is plotted in gray (95th percentile).

of Mexico and southern Chile, though it cannot be measured from the available data set. Site factors from two criteria vary less and are within ±20%.

Considering these error estimations and the fact that the errors from the first test are very small, we consider the overall error of estimation in this study to be ±0.002 for the attenuation parameter C and ±20% for site factors, with larger uncertainty for Mexico and southern Chile.

Synthetic Tests for Distance-Dependent Attenuation Parameter from Tectonic Tremor

Our estimation of the attenuation parameter is dependent on the distance limit. To understand the source of this dependence, we create synthetic data and perform the same analysis to estimate C and the relative site factors. We consider two different attenuation structures to determine if the observed distance-dependent C is due to a layered attenuation model. The first, a reference model, is that of Katsumata (2001), which represents the average attenuation structure in Japan. In this model, the upper layer, with a thickness of 20 km and shear-wave attenuation, Q_S of 500, is less attenuating than the lower layer, with a thickness of 10 km and $Q_S = 100$ (Fig. 10a). The second attenuation model we consider is the opposite; that is, the shallower layer is thinner (10 km) and more attenuating, with $Q_S = 200$, and the deeper layer is thicker (20 km) and less attenuating with $Q_S = 1000$ (Fig. 10b).

We next generate synthetic PGV data by considering 2000 tremor sources at 30 km depth recorded by six surface stations. The logarithms of source parameters, $\log(\text{Source}_i)$, for the 2000 sources are uniform-randomly defined within the range of 9.0–11.0, which is slightly larger than the source terms in the Nankai region (Fig. 5) due to strong attenuation of the first model. Similarly, site factors are uniform-randomly defined between 0.5 and 1.5 for each calculation, with the reference stations set at 1.00 and the noise level set at 30 nm/s at all stations. We use the velocity structure of JMA 2001 (Ueno *et al.*, 2002) to compute the ray paths. For each event–station pair, we calculate path-averaged attenuation and geometrical spreading by ray tracing and apply the site factors and source term to obtain a synthetic PGV. The ray path (i.e., epicentral distance) for each event–station pair is randomly chosen from 8990 ray paths having incident angle from 0° to 89.9°. To mimic noise in real data, the PGV is multiplied by a random number having a uniform distribution from 0.8 to 1.2. Furthermore, 1% of PGV are replaced by a random value from 100 to 1600 nm/s, which captures the effect of random noise.

Figure 10a shows the synthetic PGV data generated using the attenuation structure of Katsumata (2001), the estimated C and site factors for the different distance limits, and synthetic path-averaged attenuation for specific hypocentral distance. The site factors are stable and well reproduced in this estimation. The obtained attenuation parameter is smaller when using only close data, whereas it is larger when using a greater distance limit that includes more data. This dependence of the attenuation parameter on the distance limit is opposite to what we observe with data, as in Figure 4, in which C decreases with increasing distance before becoming stable. Furthermore, the absolute value of C, near 0.031, is much larger than the C obtained from actual tremor data. With the second attenuation structure, a less-attenuating deep layer, however, the results show a dependence of C on distance that is more similar to the data results, in which the parameter is large at smaller distance before becoming stable at greater distance (Fig. 10b). This final value of C is similar to the results found from the

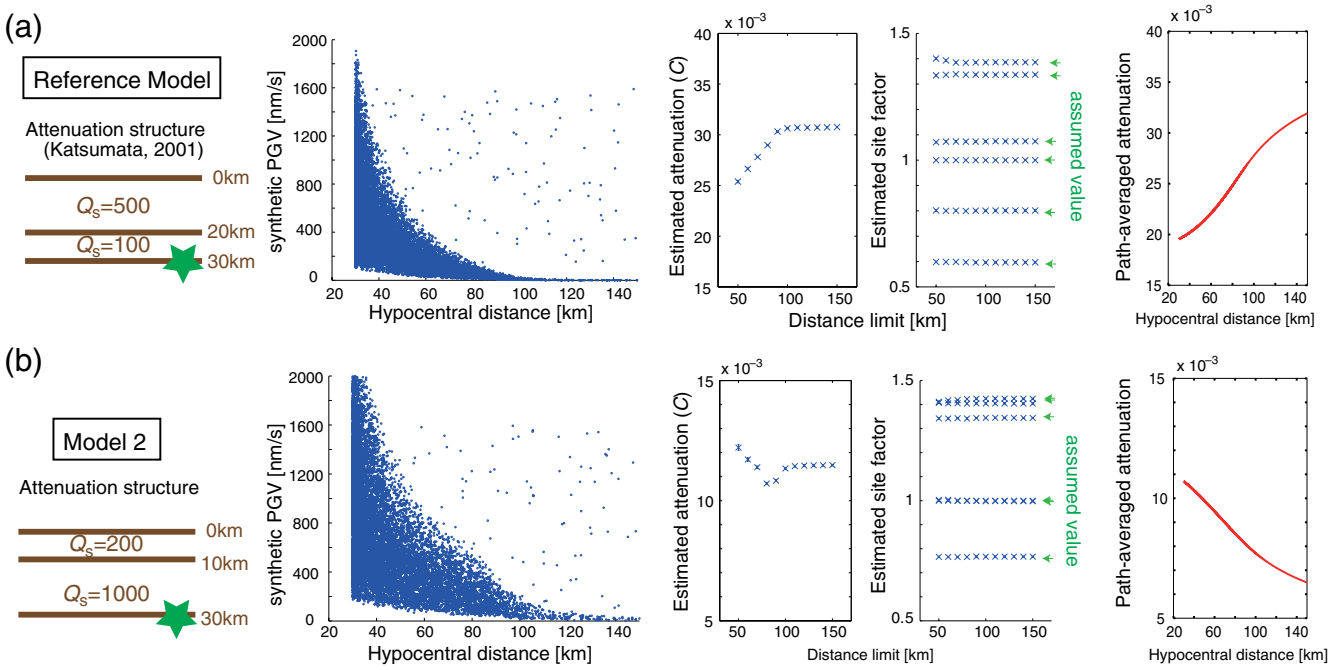

Figure 10. Synthetic tests for seismic attenuation are conducted at the source depth of tectonic tremor. (a) Seismic attenuation structure assumed by Katsumata (2001) (left panel). Calculated synthetic data (second panel) using this structure and method as explained in the text, and estimated C and site factors (third panel). In the site factor plot, the arrows are drawn at the level assumed when calculating synthetic data; the site factors are well reproduced in the synthetic study. In the most right panel, synthetic path-averaged attenuation for specific hypocentral distance calculated from assumed attenuation structure is shown. (b) Same as (a) for model 2. The color version of this figure is available only in the electronic edition.

actual tremor data, because the second attenuation model was chosen to match the actual values by trial and error.

The attenuation parameter C obtained in this analysis is the path-averaged attenuation. When using only the PGV data with small hypocentral distances, the ray paths are nearly vertical, and the distance of the seismic waves in each layer is nearly equal to the thickness of that layer. On the other hand, when the hypocentral distances become larger, the ray paths are more oblique in the deeper layer. The distance traveled by this oblique ray path in the deeper layer is longer, but the distance traveled in the shallower layer is similar to that for small hypocentral distances, due to ray-path bending. Therefore, for the larger distances, the deeper layer has more influence on the attenuation. In the right panel of Figure 10, we calculate synthetic C values at specific hypocentral distances (rather than for a distance limit) for each model so the estimated C for each distance limit is the average of the synthetic attenuation for all distances less than that distance limit. In the reference model, the deeper layer has stronger attenuation, resulting in increasing synthetic attenuation with hypocentral distance (Fig. 10a). On the other hand, for model 2, with weaker attenuation in the deep layer, a decreasing synthetic attenuation with hypocentral distance is found (Fig. 10b). The estimated C value for both models (third panel of Fig. 10) is slightly larger than the average of the synthetic value within each distance limit (far right panel), perhaps due to the limitation of the assumption that geometrical spreading is represented as $1/R$. This deviation is also within the range of error of the attenuation parameter.

This forward-modeling approach demonstrates that an increasing C with distance implies a more-attenuating deep and less-attenuating shallower layer, whereas a decreasing C with distance implies that the shallower layer is more attenuating. As Figure 4 exhibits, the actual tremor data show a decreasing trend in attenuation with larger distance limits for all of the regions considered, matching model 2. This indicates that the shallower layer of the upper plate of these various subduction zones is more attenuating than the deeper layer.

Synthetic Tests for Distance Dependent Attenuation Parameter from Intraslab Earthquakes

In the Nankai subduction zone, the attenuation parameter values estimated for intraslab earthquakes are significantly larger than those estimated from tremor (Fig. 6). Because we have band-pass filtered both data sets between 2 and 8 Hz, the attenuation parameter should only be affected by the path and is not source dependent. The major difference between tectonic tremor and intraslab earthquakes in Nankai is the source depth, so it is likely that the material at depths between the tremor event hypocenters and intraslab earthquake hypocenters has a characteristic attenuation that affects our estimation of C. Based on this idea, we construct a simple layered attenuation structure (Fig. 11a) by trial-and-error modeling that explains the differences in attenuation. In this model, we keep

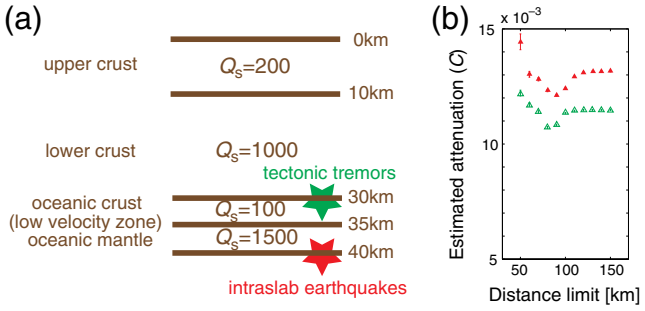

Figure 11. Synthetic test for seismic attenuation is conducted at the source depth of intraslab earthquakes, analogous to that of tremor in Figure 10. (a) The seismic attenuation structure assumed using model 2 (Fig. 10b), with an additional attenuating 5 km thin layer to represent oceanic crust and a 5 km less-attenuating layer to represent the oceanic mantle. (b) Seismic attenuation (C) is determined from synthetic data for intraslab earthquakes using the attenuation structure in (a), assumed for the seismic source to be located at 40 km depth. Open triangles show the result for tectonic tremors (same as the plot in Figure 10b), and solid triangles show results for intraslab earthquakes. The color version of this figure is available only in the electronic edition.

the shallower two layers the same as that of model 2 in Figure 10b, set $Q_S = 100$ from 30 to 35 km depth to simulate the subducting and strongly attenuating oceanic crust, and set $Q_S = 1500$ (i.e. nearly lossless) from 35 to 40 km depth to simulate the subducting oceanic mantle (Katsumata, 2001). The S-wave velocity in the attenuating layer (between 30 and 35 km depth) is set at 3.6 km/s (about a 10% reduction from the JMA 2001; Hirose *et al.*, 2008). We calculate synthetic PGV data in the same manner as the previous section with this structure and source depth for intraslab earthquakes of 40 km, and we estimate C for different distance limits.

We compare the estimated values of C from tectonic tremor and intraslab earthquakes in Figure 11b. The estimated C for intraslab earthquakes is larger, due to the introduction of highly attenuating oceanic crust. This synthetic test implies that we can estimate a difference in C if there is an attenuating layer between tectonic tremors and intraslab earthquakes, even if that attenuating layer is only 5 km thick.

Tectonic tremor, due to the depth and low-angle thrust mechanism of low-frequency earthquakes, which comprise tremor, are considered to occur on the plate interface (Ide, Shelly, and Beroza, 2007; Royer and Bostock, 2013), whereas intraslab earthquakes are located near the oceanic Moho (e.g., Shelly *et al.*, 2006). Therefore, oceanic crust separates the two populations of earthquakes. This crust is thought to be a low-velocity and high V_P/V_S region (Shelly *et al.*, 2006; Hirose *et al.*, 2008; Audet *et al.*, 2009; Kato *et al.*, 2010) with strong attenuation (Eberhart-Phillips *et al.*, 2005; Reyners and Eberhart-Phillips, 2009; Takaoka *et al.*, 2012; Kita *et al.*, 2013), which may be attributable to the existence of high fluid pressure or hydrous minerals in the oceanic crust.

In the Nankai subduction zone, from Tokai to Shikoku, Hirose *et al.* (2008) have imaged a layer of about 5 km in thickness with a low V_S and high V_P/V_S. The intraslab earthquakes of the Philippine Sea plate are located just below this layer, which is consistent with our model of the attenuation structure in Figure 11a. The observed difference in C values between tremor and intraslab earthquakes is significant, given our estimated error, and is therefore attributable to the subducting Philippine Sea plate, which is assumed in our model to have $Q_S = 100$. The actual value of Q_S is difficult to estimate due to strong trade-offs between Q_S and the layer thickness, but we can say that it is significantly more attenuating than the other layers.

Table 2
Summary of Results and Previous Studies

Region	Study	Data Type	Typical C	Frequency	Minimum C	Maximum C
Shikoku	This study	Tremor	0.008	PGV*	0.004	0.012
		Intraslab	0.016	PGV	—	—
Kii	This study	Tremor	0.010	PGV	0.002	0.012
		Intraslab	0.016	PGV	—	—
Tokai	This study	Tremor	0.006	PGV	0.004	0.009
		Intraslab	0.012	PGV	—	—
Shikoku-Kii	Fukushima *et al.* (2000)	Crust	0.0076	PGV	—	—
Japan	Si and Midorikawa (2000)	Crust/Interplate/Intraslab	—	—	0.0046 (PGV)	0.0069 (PGA†)
Japan	Kanno *et al.* (2006)	Depth < 30 km	0.0037	2 Hz	0.0021 (PGV)	0.0092 (8 Hz)
		Depth > 30 km	0.0074	PGV	0.0069 (2 Hz)	0.0101 (8 Hz)
Cascadia	This study	Tremor	0.005	PGV	0.002	0.006
Cascadia	Baltay and Beroza (2013)	Tremor	0.00471	PGV	0.00467	0.00480
Cascadia	Atkinson and Boore (1997)	Crust/Intraslab	0.00414	2 Hz	0.00254 (PGV)	0.00783 (8 Hz)
Jalisco	This study	Tremor	0.009	PGV	0.004	0.010
Mexico	García *et al.* (2005)	Intraslab	0.0055	2 Hz	0.0053 (PGV)	0.0085 (5 Hz)
S. Chile	This study	Tremor	0.006	PGV	0.003	0.007
N. Chile	Boroschek and Contreras (2012)	Interplate	—	—	0.0018 (2 Hz)	0.0044 (10 Hz)

*PGV, peak ground velocity.
†PGA, peak ground acceleration.

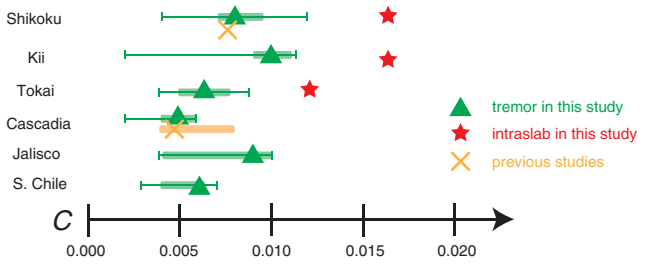

Figure 12. Compiled results of the seismic attenuation parameter C from this study and other studies. Triangles represent estimated C from tectonic tremors found in this study, with error bars showing the range of values. The thick bars indicate the range from the second minimum to the second maximum of the estimated C in the station dependency test (Fig. 8), whereas the thin bars show the minimum and maximum estimated C. Stars in the Shikoku, Kii, and Tokai regions show estimated C from intraslab earthquakes. Crosses and their associated thick bars give the range of C estimated by previous studies in the same region (Fukushima *et al.*, 2000, in Shikoku; Baltay and Beroza, 2013 [bar], and Atkinson and Boore, 1997 [cross] in Cascadia). The color version of this figure is available only in the electronic edition.

Comparison with Previous Studies

The purpose of this study is to estimate the C for implementation into GMPEs in subduction zone regions where typical earthquake records are sparse. We use a distance limit of 150 km for our final values of C, determined for PGV from tectonic tremor, and compare it to previous studies (Table 2 and Fig. 12). Some previous studies do not consider attenuation from PGV, and it is not clear how directly PGV from tremor corresponds in our frequency band to PGV from earthquakes used in these previous studies. We expect PGV to be generated from frequencies near the corner frequency of large events, which will be lower than the 2–8 Hz range that we are considering with tremor. Because of these considerations, it may be more applicable to compare our attenuation parameters, found in the range of 2–8 Hz, with spectral acceleration values from the previous studies in the 2–8 Hz range. Although some studies performed their analysis in $\log_{10}$, this study uses the natural logarithm, so we re-express the values from other researchers in natural logarithm for consistency.

Fukushima *et al.* (2000) find $C = 0.0076$ in Japan and are able to fit the ground motion from the 1995 Kobe earthquake well with their GMPE. Because the Kobe is a crustal earthquake, which occurred near the Shikoku region, it should be consistent with our C from tectonic tremor; our value of 0.008 matches theirs well. Si and Midorikawa (2000) *a priori* assume $C = 0.0046$ for PGV. Because they do not discuss whether their result is based on crustal, inter-, or intraplate events, it may simply be representative of an overall averaged value, while our value is for plate-interface events.

Kanno *et al.* (2006) estimate attenuation parameters for shallow (depth < 30 km) and deep (depth > 30 km) earthquakes in Japan. Because our tremor sources are assumed to be located at 30 km depth, we expect our attenuation parameter values to be between those of Kanno *et al.* (2006) for shallow and deep events. For PGV, they find C parameters of 0.0021 and 0.0074 for shallow and deep sources, respectively. For spectral acceleration frequencies ranging between 2 and 8 Hz, their C values are between 0.0037 and 0.0092 for shallow events and 0.0069 and 0.0101 for deep events. Our median attenuation parameters for the Nankai region range from 0.006 to 0.010, so our results are consistent overall with those of Kanno *et al.* (2006). However, their deep earthquakes are mainly in the Tohoku and Hokkaido regions of Japan, so we cannot directly compare their deep results with ours. They do find that deeper earthquakes, some of which would be intraslab, tend to have larger C values than shallower events, which is consistent with our result in the Nankai region.

Nakamura and Uetake (2002) and Pei *et al.* (2009) estimated the seismic attenuation structure in Japan by conducting Q tomography. In those studies, the Shikoku region tends to be more attenuating than the Kii and Tokai regions. Here, we find the estimated attenuation parameter in Shikoku to be larger than that of Tokai, in agreement with the Q-tomography studies. In the Kii region, our estimated C is large, but this region also shows large station variability (Fig. 8). As discussed earlier, the large station variability may represent local variations, which seems to be consistent with the result of Pei *et al.* (2009). Overall, the regional variations of attenuation characteristics in the Nankai subduction zone that we find are consistent with previous studies.

In Cascadia, Baltay and Beroza (2013) investigated seismic attenuation from tectonic tremors using a similar method. They found a C value for PGV between 0.00467 and 0.00480, which is very similar to our result of 0.005. The GMPE from Atkinson and Boore (1997) for the Cascadia region for both crustal and intraslab earthquakes has $C = 0.0025$ for PGV from ordinary earthquakes, which is smaller than our estimated attenuation parameter. They also find attenuation parameters for spectral acceleration ranging from 0.0041 at 2 Hz to 0.008 at 8 Hz. They do not distinguish intraslab earthquakes from crustal earthquakes for analysis, which might result in a slightly higher estimated C value; however, our attenuation parameter in Cascadia of $\sim$0.005 for PGV is between their attenuation values of 0.004 and 0.008 at 2 and 8 Hz, so is consistent with those results.

In Mexico, García *et al.* (2005) developed a GMPE for the broader Mexican subduction zone region and found C values for PGV of 0.0053 and spectral accelerations of 0.0055 for 2 Hz and 0.0085 for 5 Hz. In the Jalisco region, Tejeda-Jácome and Chávez-García (2007) developed a GMPE but do not take seismic attenuation and scattering (our C parameter) explicitly into account. Our average value for $C = 0.009$ in Jalisco is not far from that of García *et al.* (2005), but, as their region is much larger, we may be able to resolve smaller scale variations that give rise to slightly different attenuation values.

Along the South American subduction zone in Chile, there is little regular seismic activity, but many ordinary earthquakes occur 1000–3000 km farther north. Using interplate earthquakes in that area, Boroschek and Contreras (2012) estimate a C parameter of 0.0018 and 0.0044 for spectral accelerations at 2 and 10 Hz, respectively. These values are similar to our average C value of 0.006. However, these regions are disparate, and hence we cannot directly compare their result with ours. In southern Chile near the triple junction, our study provides the first estimate of the GMPE attenuation parameter.

Some studies listed here do not distinguish between crustal, interplate, and intraslab earthquakes when developing GMPEs. However, our study shows that intraslab earthquakes give rise to a larger C than do interplate events due to their location below the subducting oceanic crust. This trend can be also seen in the work of Kanno *et al.* (2006). If we use an attenuation parameter obtained from intraslab earthquakes to predict ground motion of interplate earthquakes, that ground motion may be underestimated, an unwelcome trend given the location of mega-interplate earthquakes. Plate-interface earthquakes alone should be used to estimate GMPE parameters for seismic-hazard maps and assessments.

In this study, we have shown that tectonic tremor can be used to determine the attenuation parameter for GMPEs in regions where ordinary earthquakes may not often occur. Physically, tectonic tremor tends to occur in regions where ordinary earthquakes are less likely (e.g., Ide, 2013), so their seismic signals are a helpful tool to estimate attenuation in these areas. The results of this study for the C parameter and its range of reliability are schematically summarized in Figure 12, and the comparisons to other studies are given in Table 2.

Discussion

The seismic attenuation parameter in the subducting plate as determined using tectonic tremor differs, with statistical significance, between subduction zones (Fig. 12). The cause of this variation in attenuation is still unclear, but physical controls might be the age of the subducting plate, as temperature affects attenuation (e.g., Karato, 2003); however, the subducting oceanic plates in this study all have similar ages. An alternative explanation is that the material constituting the continental crust might exert an influence on the seismic attenuation in the crust.

The highly attenuating subducting oceanic crust, which is often the host of the tremor source region, has been imaged in several studies, yet the results are not conclusive (Eberhart-Phillips *et al.*, 2005; Reyners and Eberhart-Phillips, 2009; Takaoka *et al.*, 2012; Kita *et al.*, 2013). Smoothing and limited resolution, typically 10–20 km, in Q tomography make it difficult to identify an attenuating layer as thin as ~5 km. We have inferred such a layer through comparison of attenuation between tectonic tremors and intraslab earthquakes with different hypocentral depths. Obtaining actual Q values of oceanic crust requires a more sophisticated analysis that models specific frequencies and careful event location selection of tremors and intraslab earthquakes so that path effects in the upper plate are canceled, as well as consideration of different geometrical spreading coefficients (i.e., different from -1). We also note that the estimated C in our study includes both anelastic attenuation and scattering, so to obtain an intrinsic Q value for the oceanic crust, the effect of scattering must be estimated (e.g., Takemura and Yoshimoto, 2014).

The strongly attenuating oceanic crust suggested in this study adds to the evidence for pore fluids caused by dehydration reactions in the subducting slab in the tremor source region. Tremor activity has various heterogeneities, such as tidal sensitivity, duration of signal, and recurrence interval (e.g., Obara *et al.*, 2010; Wech and Creager, 2011; Ide, 2012) that might be influenced by the amount of dehydrated fluid. Takaoka *et al.* (2012) show that oceanic crust at depths below the tremor source is less attenuating, which may be due to the lack of the dehydration reactions. Thus, the amount of dehydrated fluid could, in principle, be estimated from the variation in seismic attenuation as determined in this study.

Conclusion

We estimate seismic attenuation using tectonic tremor in the Nankai, Cascadia, Jalisco, and southern Chile subduction zones, quantitatively estimating the attenuation parameter C and relative site factors for application in GMPEs. The estimated attenuation parameters vary between regions, which may be indicative of the material constituting the overriding plate. By estimating the distance dependence of the attenuation parameter, using several distance limits, we show that the shallower layer of the upper plate is more attenuating than the deeper layer. We also apply the same method to estimate attenuation from intraslab earthquakes (which occur near the oceanic Moho) to demonstrate that oceanic crust (which exists in a layer between tectonic tremor and intraslab earthquakes) has strong attenuation. These results caution against the use of intraslab earthquakes for ground-motion prediction because they may overestimate the effects of attenuation on predicted ground motion from megathrust earthquakes. Our method can be employed to estimate the attenuation parameter in subduction zones where ordinary earthquakes on the plate interface do not often occur and hence where GMPEs are poorly constrained.

Data and Resources

The earthquake catalog is provided by Japan Meteorological Agency (JMA) for the Nankai region and by Universidad Nacional Autonoma de Mexico (UNAM) for the Mexico subduction zone. The seismic waveforms are downloaded from Hi-net, maintained by the National Research Institute for Earth Science and Disaster Prevention (NIED) for Shikoku, Kii, and Tokai regions; from the Plate Boundary

Observatory through Incorporated Research Institutions for Seismology (IRIS) and the Canadian National Seismograph Network through CNDC for Cascadia; through IRIS from the "Mapping the Rivera Subduction Zone" project for Jalisco; and through IRIS from the Chile Ridge Subduction Network in southern Chile. Some figures in this study are drawn using Generic Mapping Tools software (Wessel and Smith, 1995).

Acknowledgments

The authors appreciate all data sources listed above. We also appreciate useful comments from H. Miyake in the Earthquake Research Institute at the University of Tokyo. We appreciate two anonymous reviewers for providing helpful comments to improve this manuscript. This work was supported by Japan Society for the Promotion of Science KAKENHI (23244090), Ministry of Education, Culture, Sports, Science, and Technology (MEXT) KAKENHI (21107007), the Program for Leading Graduate Schools, MEXT, Japan.

References

Ando, M. (1975). Source mechanisms and tectonic significance of historical earthquakes along the Nankai trough, Japan, *Tectonophysics* **27,** no. 2, 119–140, doi: 10.1016/0040-1951(75)90102-X.

Atkinson, G. M., and D. M. Boore (1997). Stochastic point-source modeling of ground motions in the Cascadia region, *Seismol. Res. Lett.* **68,** no. 1, 74–85, doi: 10.1785/gssrl.68.1.74.

Audet, P., M. G. Bostock, N. I. Christensen, and S. M. Peacock (2009). Seismic evidence for overpressured subducted oceanic crust and megathrust fault sealing, *Nature* **457,** 76–78, doi: 10.1038/nature07650.

Baltay, A., and G. Beroza (2013). Ground motion prediction from tremor, *Geophys. Res. Lett.* **40,** 1–6, doi: 10.1002/2013GL058506.

Boatwright, J., and L. Seekins (2011). Regional spectral analysis of three moderate earthquakes in northeastern North America, *Bull. Seismol. Soc. Am.* **101,** no. 4, 1769–1782, doi: 10.1785/0120100225.

Boore, D. M., and W. B. Joyner (1982). The empirical prediction of ground motion, *Bull. Seismol. Soc. Am.* **72,** no. 6B, S43–S60.

Boroschek, R., and V. Contreras (2012). Strong ground motion from the 2010 M_w 8.8 Maule Chile earthquake and attenuation relations for Chilean subduction zone interface earthquakes, in *International Symposium on Engineering Lessons Learned from the 2011 Great East Japan Earthquake*, Tokyo, Japan, 1–4 March 2012, Vol. 1, 1722–1733.

Chapman, J. S., and T. I. Melbourne (2009). Future Cascadia megathrust rupture delineated by episodic tremor and slip, *Geophys. Res. Lett.* **36,** L22301, doi: 10.1029/2009GL040465.

Dantzig, G. B., A. Orden, and P. Wolfe (1955). The generalized simplex method for minimizing a linear form under linear inequality restraints, *Pac. J. Math.* **5,** no. 2, 183–195.

Eberhart-Phillips, D., D. H. Han, and M. D. Zoback (1989). Empirical relationships among seismic velocity, effective pressure, porosity, and clay content in sandstone, *Geophysics* **54,** no. 1, 82–89, doi: 10.1190/1.1442580.

Eberhart-Phillips, D., M. Reyners, M. Chadwick, and J. M. Chiu (2005). Crustal heterogeneity and subduction processes: 3-D V_P, V_P/V_S and Q in the southern North Island, New Zealand, *Geophys. J. Int.* **162,** no. 1, 270–288, doi: 10.1111/j.1365-246X.2005.02530.x.

Fukushima, Y., K. Irikura, T. Uetake, and H. Matsumoto (2000). Characteristics of observed peak amplitude for strong ground motion from the 1995 Hyogoken Nanbu (Kobe) earthquake, *Bull. Seismol. Soc. Am.* **90,** no. 3, 545–565, doi: 10.1785/0119990066.

García, D., S. K. Singh, M. Herráiz, M. Ordaz, and J. F. Pacheco (2005). Inslab earthquakes of central Mexico: Peak ground-motion parameters and response spectra, *Bull. Seismol. Soc. Am.* **95,** no. 6, 2272–2282, doi: 10.1785/0120050072.

Hacker, B. R., S. M. Peacock, G. A. Abers, and S. D. Holloway (2003). Subduction factory 2. Are intermediate-depth earthquakes in subducting slabs linked to metamorphic dehydration reactions? *J. Geophys. Res.* **108,** no. B1, 2030, doi: 10.1029/2001JB001129.

Hirose, F., J. Nakajima, and A. Hasegawa (2008). Three-dimensional seismic velocity structure and configuration of the Philippine Sea slab in southwestern Japan estimated by double-difference tomography, *J. Geophys. Res.* **113,** no. B09315, doi: 10.1029/2007JB005274.

Ide, S. (2010). Striations, duration, migration, and tidal response in deep tremor, *Nature* **466,** 356–359, doi: 10.1038/nature09251.

Ide, S. (2012). Variety and spatial heterogeneity of tectonic tremor worldwide, *J. Geophys. Res.* **117,** no. B03302, doi: 10.1029/2011JB008840.

Ide, S. (2013). The proportionality between relative plate velocity and seismicity in subduction zones, *Nat. Geosci.* **6,** 780–784, doi: 10.1038/ngeo1901.

Ide, S., G. C. Beroza, D. R. Shelly, and T. Uchide (2007). A scaling law for slow earthquakes, *Nature* **447,** 76–79, doi: 10.1038/nature05780.

Ide, S., D. R. Shelly, and G. C. Beroza (2007). Mechanism of deep low frequency earthquakes: Further evidence that deep non-volcanic tremor is generated by shear slip on the plate interface, *Geophys. Res. Lett.* **34,** L03308, doi: 10.1029/2006GL028890.

Kanno, T., A. Narita, N. Morikawa, H. Fujiwara, and Y. Fukushima (2006). A new attenuation relation for strong ground motion in Japan based on recorded data, *Bull. Seismol. Soc. Am.* **96,** no. 3, 879–897, doi: 10.1785/0120050138.

Karato, S. (2003). Mapping water content in the upper mantle, in *Inside the Subduction Factory*, J. Eiler (Editor), American Geophysical Monograph 138, 135–152, doi: 10.1029/138GM08.

Kato, A., T. Iidaka, R. Ikuta, Y. Yoshida, K. Katsumata, T. Iwasaki, S. Sakai, C. Thurber, N. Tsumura, K. Yamaoka, T. Watanabe, T. Kunitomo, F. Yamazaki, M. Okubo, S. Suzuki, and N. Hirata (2010). Variations of fluid pressure within the subducting oceanic crust and slow earthquakes, *Geophys. Res. Lett.* **37,** L14310, doi: 10.1029/2010GL043723.

Katsumata, A. (2001). Magnitude determination of deep-focus earthquakes in and around Japan with regional velocity-amplitude data, *Earth Planet. Space* **53,** no. 5, 333–346.

Kita, S., J. Nakajima, T. Okada, A. Hasegawa, K. Katsumata, Y. Asano, and N. Uchida (2013). High-resolution seismic attenuation structure beneath Hokkaido corner, northern Japan, *Eos Trans. AGU* (Fall Meet.), Abstract S23A–2472.

Liu, Z., S. Owen, D. Dong, P. Lundgren, F. Webb, E. Hetland, and M. Simons (2010). Estimation of interplate coupling in the Nankai trough, Japan using GPS data from 1996 to 2006, *Geophys. J. Int.* **181,** no. 3, 1313–1328, doi: 10.1111/j.1365-246X.2010.04600.x.

Mehrotra, S. (1992). On the implementation of a primal-dual interior point method, *SIAM J. Optim.* **2,** no. 4, 575–601, doi: 10.1137/0802028.

Menke, W. (1989). *Geophysical Data Analysis: Discrete Inverse Theory*, Academic Press Inc., San Diego, California, 79–101.

Miyazawa, M., and J. Mori (2005). Detection of triggered deep low-frequency events from the 2003 Tokachi-Oki earthquake, *Geophys. Res. Lett.* **32,** L10307, doi: 10.1029/2005GL022539.

Miyoshi, T., and K. Obara (2010). Double seismic zone within the ridge-shaped slab beneath southwest Japan, *Earth Planet. Space* **62,** no. 12, 949.

Nakamura, R., and T. Uetake (2002). Three dimensional attenuation structure and site amplification inversion by using a large quantity of seismic strong motion records in Japan, *Zisin* **54,** 475–488.

Obana, K., S. Kodaira, and Y. Kaneda (2005). Seismicity in the incoming/subducting Philippine Sea plate off the Kii Peninsula, central Nankai trough, *J. Geophys. Res.* **110,** no. B11311, doi: 10.1029/2004JB003487.

Obara, K. (2002). Nonvolcanic deep tremor associated with subduction in southwest Japan, *Science* **296,** 1679–1681, doi: 10.1126/science.1070378.

Obara, K., S. Tanaka, T. Maeda, and T. Matsuzawa (2010). Depth-dependent activity of non-volcanic tremor in south- west Japan, *Geophys. Res. Lett.* **37,** L13306, doi:10.1029/2010GL043679.

Park, J. O., T. Tsuru, N. Takahashi, T. Hori, S. Kodaira, A. Nakanishi, S. Miura, and Y. Kaneda (2002). A deep strong reflector in the Nankai accretionary wedge from multichannel seismic data: Implications for underplating and interseismic shear stress release, *J. Geophys. Res.* **107,** no. B4, doi: 10.1029/2001JB000262.

Peacock, S. M., and K. Wang (1999). Seismic consequences of warm versus cool subduction metamorphism: Examples from southwest and northeast Japan, *Science* **286,** 937–939, doi: 10.1126/science.286.5441.937.

Pei, S., Z. Cui, Y. Sun, M. N. Toksöz, C. A. Rowe, X. Gao, J. Zhao, H. Liu, J. He, and F. D. Morgan (2009). Structure of the upper crust in Japan from *S*-wave attenuation tomography, *Bull. Seismol. Soc. Am.* **99,** no. 1, 428–434, doi: 10.1785/0120080029.

Reyners, M., and D. Eberhart-Phillips (2009). Small earthquakes provide insight into plate coupling and fluid distribution in the Hikurangi subduction zone, New Zealand, *Earth. Planet. Sci. Lett.* **282,** no. 1, 299–305, doi: 10.1016/j.epsl.2009.03.034.

Rogers, G., and H. Dragert (2003). Episodic tremor and slip on the Cascadia subduction zone: The chatter of silent slip, *Science* **300,** 1942–1943, doi: 10.1126/science.1084783.

Royer, A. A., and M. G. Bostock (2013). A comparative study of low frequency earthquake templates in northern Cascadia, *Earth. Planet. Sci. Lett.*, doi: 10.1016/j.epsl.2013.08.040.

Satake, K., K. Shimazaki, Y. Tsuji, and K. Ueda (1996). Time and size of a giant earthquake in Cascadia inferred from Japanese tsunami records of January 1700, *Nature* **379,** 246–249, doi: 10.1038/379246a0.

Shelly, D. R., G. C. Beroza, and S. Ide (2007). Complex evolution of transient slip derived from precise tremor locations in western Shikoku, Japan, *Geochem. Geophys. Geosys.* **8,** Q10014, doi: 10.1029/2007GC001640.

Shelly, D. R., G. C. Beroza, S. Ide, and S. Nakamula (2006). Low-frequency earthquakes in Shikoku, Japan, and their relationship to episodic tremor and slip, *Nature* **442,** 188–191, doi: 10.1038/nature04931.

Si, H., and S. Midorikawa (2000). New attenuation relations for peak ground acceleration and velocity considering effects of fault type and site condition, in *Proc. of Twelfth World Conference on Earthquake Engineering*, Auckland, New Zealand, 20 January–4 February 2000, paper number 0532.

Takaoka, H., N. Tsumura, H. Takahashi, K. Nozaki, A. Kato, T. Iidaka, T. Iwasaki, S. Sakai, N. Hirata, R. Ikuta, T. Kunitomo, Y. Yoshida, K. Katsumata, K. Yamaoka, T. Watanabe, F. Yamazaki, M. Okubo, and S. Suzuki (2012). Three-dimensional attenuation structure beneath the Tokai region, central Japan derived using local earthquake spectra, *Zisin* **65,** no. 2, 175–187.

Takemura, S., and K. Yoshimoto (2014). Strong seismic wave scattering in the low-velocity anomaly associated with subduction of oceanic plate, *Geophys. J. Int.* **197,** no. 2, 1016–1032, doi: 10.1093/gji/ggu031.

Takemura, S., T. Furumura, and T. Saito (2009). Distortion of the apparent *S*-wave radiation pattern in the high-frequency wavefield: Tottori-ken Seibu, Japan, earthquake of 2000, *Geophys. J. Int.* **178,** no. 2, 950–961, doi: 10.1111/j.1365-246X.2009.04210.x.

Tejeda-Jácome, J., and F. J. Chávez-García (2007). Empirical ground-motion estimation equations in Colima from weak motion records, *ISET J. Earthq. Technol.* **44,** nos. 3/4, 409–420.

Thomas, A. M., R. M. Nadeau, and R. Bürgmann (2009). Tremor-tide correlations and near-lithostatic pore pressure on the deep San Andreas fault, *Nature* **462,** no. 7276, 1048–1051, doi: 10.1038/nature08654.

Ueno, H., S. Hatakeyama, T. Aketagawa, J. Funasaki, and N. Hamada (2002). Improvement of hypocenter determination procedures in the Japan Meteorological Agency, *Q. J. Seismol.* **65,** 123–134.

Wech, A. G., and K. C. Creager (2011). A continuum of stress, strength and slip in the Cascadia subduction zone, *Nat. Geosci.* **4,** no. 9, 624–628, doi: 10.1038/ngeo1215.

Wessel, P., and W. H. Smith (1995). New version of the Generic Mapping Tools, *Eos Trans. AGU* **76,** no. 33, 329.

Winkler, K. W., and W. F. Murphy (1995). Acoustic velocity and attenuation in porous rocks, in *Rock Physics and Phase Relations: A Handbook of Physical Constants*, T. J. Ahrens (Editor), American Geophysical Union, Washington, D.C., 20–34.

Zhang, Y. (1998). Solving large-scale linear programs by interior-point methods under the MATLAB Environment, *Optim. Meth. Software.* **10,** no. 1, 1–31, doi: 10.1080/10556789808805699.

The Department of Earth and Planetary Science
The University of Tokyo
7-3-1 Hongo, Bunkyo-ku
Tokyo 113-0033, Japan
yabe@eps.s.u-tokyo.ac.jp
ide@eps.s.u-tokyo.ac.jp
(S.Y., S.I.)

Earthquake Science Center
USGS Menlo Park
345 Middlefield Rd
Menlo Park, California 94025
abaltay@usgs.gov
(A.S.B.)

The Department of Geophysics
Stanford University
397 Panama Mall
Stanford, California 94305
beroza@stanford.edu
(G.C.B.)

Manuscript received 3 February 2014;
Published Online 15 July 2014